IJBBE International Journal of Biophotonics & Biomedical Engineering Vol. 5, No. 1, Spring-Summer, 2025

Research Article

Optical biosensor for detection of hemoglobin using ternary photonic crystals

M. Aghamohammadian [a], A. Vahedi[*, b], and S. Haghipour [a]

[a] Department of Medicine Engineering, Ta.C., Islamic Azad University, Tabriz, Iran
[b] Department of Physics, Ta.C., Islamic Azad University, Tabriz, Iran

***Corresponding Author Email: minooaghamohammadian74@gmail.com**

DOI: 10.71498/ijbbe.2025.1193386

ABSTRACT

Received: Dec. 13, 2024, Revised: May. 16, 2025, Accepted: May. 28, 2025, Available Online: Jul. 24, 2025

Optical biosensors have attracted the attention of researchers because they have a unique ability to control the dispersal of photons and detect the natural shape of biomolecules. The main component of blood is hemoglobin, whose main function is to transport oxygen to body tissues and remove carbon dioxide from them. This article aims to simulate biosensors that can detect hemoglobin concentration using photonic crystals. For this purpose, we have used two structures with $TiN/m/TiO_2$ and $Al_XGa_{1-X}N/m/TiO_2$. The m layer is a dielectric such as glass or air, which has a different refractive index and can control light transmittance. Photonic crystals have a region called the photonic band gap (PBG), in which waves cannot propagate in the structure. layers inside the photonic crystal structure controlled and adjusted the defect modes and PBG properties. To find the best result, parameters such as the layer thickness, the light incident angle, and the refractive index have been optimally selected. After examining the proposed structures, it was determined that both structures are more optimal in a wide defect layer. The results show that the $TiN/m/Al_XGa_{1-X}N$ structure has optimum sensitivity (S=780.0 nm/RIU), relative sensitivity (S_R=0.729), and figure of merit (FOM=780.01/RIU) at a selected wavelength range.

KEYWORD

Hemoglobin، Photonic Crystal،Transfer Matrix Method، Optical Biosensor

I. INTRODUCTION

The peculiar features of the photonic crystal (PhC)–structure are photonic band gaps and photon localization. The photonic band gap (PBG) is the frequency range where light of certain wavelengths cannot pass through the structure. These characteristics are the result of periodic modulation of dielectric functions, which significantly changes the spectrum of electromagnetic waves passing through it [1-3]. The photonic band gap in photonic crystals depends on the refractive index and thickness of the layers, the period of the photonic crystal, and the incident angle (and polarization) of light. PhC structures are the new technology for biosensor applications. Optical biosensors are considered analytical detectors that convert chemical, physical, or biological interactions into an optical signal. To use PhC as a

biosensor, it is crucial to change its structural arrangement to produce a resonant or defect mode in the transmission spectrum. The best way to form such a resonance mode is to create defects in the structure. Based on this, many optical devices such as optical filters, switchers, and photonic crystal fibers are produced [4-6]. PhC-based biosensors can detect biotoxins, veterinary drugs, microorganisms, pesticide residues, excessive additives, heavy metal compounds, and environmental pollutants [7-13]. Hemoglobin (Hb) is the most vital component of blood, which is mainly responsible for transporting oxygen from the lungs to different body tissues and returning carbon dioxide from the tissues to the lungs. Any deviation in the blood hemoglobin concentration leads to fatal diseases, Such as polycythemia, anemia, diabetes, and thyroid dysfunction. Detection of blood hemoglobin concentration is one of the most serious and challenging concerns of medical scientists and researchers. The resonance slope in the spectrum and its change with hemoglobin concentration are the basis of our sensor design [7, 14, 15].

In recent years, further work has been done on a PhC for hemoglobin detection. El-Khozondar et al. developed a one-dimensional ternary PhC structure for hemoglobin measurement from 0 g/L to 50 g/L concentration range, and the authors achieved a reported measurement of 46/51 nm/RIU [16] A.K. Goyal et al. recently investigated a defective PhC based on the Bloch surface. By entering samples in defect regions with different concentrations, the authors calculated the angular shift and thus obtained a result of 69 deg./RIU. [17]. J. Hao and her team designed a superconductor-based, one-dimensional PhC refractive index sensor to measure different concentrations of hemoglobin in human blood, with a sensitivity of 6.85 and 6.48 μm/RIU at 80 K and 134 K [18]. Goyal et al. studied the reflectance of a one-dimensional PhC incorporating a porous defect layer for hemoglobin detection. The authors concluded the optimal sensitivity of 323 nm/RIU and FOM of 517 1/RIU, respectively [19]. H.A. Elsayed et al. reported a one-dimensional binary hemoglobin PhC sensor in which the authors used TMM to measure the shift in the resonance peak with respect to different hemoglobin concentrations and achieved a sensitivity of 167 nm/RIU [20]. Recently, K. M. Abohassan and his team have extensively investigated one-dimensional PhC structures by studying the reflection properties via TMM for various biosensing applications. [21-24].

In this work, we designed and simulated a highly sensitive biosensor structure based on 1D-PhC with a defect layer. We calculate the transmission of polarized light (s) using the transmission matrix method (TMM) to measure the transmission of the mentioned structures and study the effect of some parameters to achieve the highest performance of the sensor configuration. The proposed sensor is efficient in measuring hemoglobin concentration. Various parameters such as figure of merit index (FOM), sensitivity (S), and full width at half maximum (FWHM) have been introduced to evaluate and compare the performance of biosensors. These parameters are numerically derived and are comparable with many of the reported values of photonic crystal-based biosensors [25-30].

II. METHOD

A schematic diagram of our proposed biosensor based on a one-dimensional defect PhC is shown in Fig. 1.

Fig. **1** Schematic representation of biophotonic sensor structure

In our design, the periodic structure consistsf three different dielectri terials abeled th thickness d_1, dm, d_2 and refractive index $n_1, , n_m$ and n_2 respectively. Ternary one-dimensional structures have more exactly controlled photonic band gaps compared to binary structures. The N and D are the periodic

layer numbers and the defect layer with thickness d_l and refractive index n_l. The PhC structure is surrounded by a substrate (S) layer at one end and air at the other. The surrounding medium and PhC determine the physical and optical characteristics of the biosensor. The transfer matrix method can be used to analyze the reflectance or transmittance properties. According to Abel's theory, the periodic structure matrix of one layer, for example (a) layer, can be described by $F(a)$ matrix, [31-33].

$$F(a) = \begin{pmatrix} g_{11} & g_{12} \\ g_{21} & g_{22} \end{pmatrix} \quad (1)$$

Elements g_{11}, g_{12}, g_{21} and g_{22} represented by:

$$g_{11} = cos\,\delta_1\, cos\,\delta_2 - \frac{p_2}{p_1}\, sin\,\delta_1 \quad (2)$$

$$g_{12} = \frac{-i}{p_1} sin\,\delta_1\, cos\,\delta_2 - \frac{i}{p_2} cos\,\delta_1\, sin\,\delta_2 \quad (3)$$

$$g_{21} = -ip_1\, sin\,\delta_1\, cos\,\delta_2 - ip_2\, cos\,\delta_1\, sin\,\delta_2 \quad (4)$$

$$g_{22} = cos\,\delta_1\, cos\,\delta_2 - \frac{p_1}{p_2}\, sin\,\delta_1\, sin\,\delta_2 \quad (5)$$

That:

$$\delta_1 = \frac{2\pi d_1}{\lambda} n_1\, cos\,\theta_1$$

$$\delta_2 = \frac{2\pi d_2}{\lambda} n_2\, cos\,\theta_2 \quad (6)$$

$$p_1 = n_1\, cos\,\theta_1$$

$$p_2 = n_2\, cos\,\theta_2 \quad (7)$$

And for period N, the matrix is:

$$F(Na) = \begin{pmatrix} F_{11} & F_{12} \\ F_{21} & F_{22} \end{pmatrix} \quad (8)$$

$$F_{11} = g_{11} u_{N-1}(\Psi) - u_{N-2}(\Psi) \quad (9)$$

$$F_{12} = g_{12} u_{N-1}(\Psi) \quad (10)$$

$$F_{21} = g_{21} u_{N-1}(\Psi) \quad (11)$$

$$F_{22} = g_{22} u_{N-1}(\Psi) - u_{N-2}(\Psi) \quad (12)$$

$$\Psi = \frac{1}{2}(g_{11} + g_{22}) \quad (13)$$

$$u_N(\Psi) = \frac{(sin(N+1)\, cos^{-1}\Psi)}{\sqrt{1-\Psi^2}} \quad (14)$$

In the next step, the defect matrix (D) was employed:

$$D(d_d) = \begin{bmatrix} cos\,\delta_d & \frac{-i}{p_d} sin\,\delta_d \\ -ip_d\, sin\,\delta_d & cos\,\delta_d \end{bmatrix} \quad (15)$$

were:

$$\delta_d = \frac{2\pi d_d}{\lambda} n_d\, cos\,\theta_d$$

$$p_d = n_d\, cos\,\theta_d \quad (16)$$

The total characteristic matrix is the product of three matrices:

$$M(\omega) = (M_a M_m M_b)^N M_D (M_b M_m M_a)^N$$

$$M = \begin{pmatrix} M_{11} & M_{12} \\ M_{21} & M_{22} \end{pmatrix} \quad (17)$$

Where the first one $(MaMmMb)^N$ describes the periodic structure on the left, and the last one $(MbMmMa)^N$ describes the periodic structure on the right, and between them, there is a defect layer matrix denoted by M_D. From these three matrices, we obtain the entire characteristic matrix of the structure, which allows us to calculate the reflection and transition coefficient (r).

$$r = \frac{(M_{11} + M_{12})j_0 - (M_{21} + M_{22})}{(M_{11} + M_{12})j_0 + (M_{21} + M_{22})} \quad (18)$$

That:

$$j_0 = \sqrt{\frac{\varepsilon_0}{\mu_0}} n_0\, cos\,\theta_0 \quad (19)$$

Finally, reflectance and transmittance are represented by:

$$R=r^2 \quad (20)$$

$$T = t^2 = 1 - r^2 \quad (21)$$

we have used glass as a substrate with refractive index $n_s = 1.524$. In a perfect, defect-free photonic crystal, it is observed a pure band gap, and when a defect is introduced, it leads to the localization of the defect states and a certain mode in the reflection spectrum is obtained. An example of the defect introduced is a hemoglobin solution. Different concentrations of the refractive index of hemoglobin solution depend on its concentration, and these changes are taken from a model function from reference [34]. The efficiency of the sensor is an important factor that determines sensitivity, which can be calculated from the following equation.

$$S = \frac{\Delta \lambda_{res}}{\Delta n} \quad (22)$$

The FOM is obtained by considering the ratio of the S to the FWHM.

$$FOM = \frac{S}{\text{FWHM}} \quad (23)$$

The quality factor is also calculated from the following formula:

$$Q = \frac{RF}{\text{FWHM}} \quad (24)$$

III. Conclusion

A. *Structure 1*

The first part aims to find the optimal state of the TiN/m/Ti O_2 layer. We use an optical biosensor based on a one-dimensional photonic crystal to detect the hemoglobin concentration. In the first part, da(TiN)=100, db(TiO_2) = 109 *and* dm thicknesses are 0, 60 and100 nm, N=3, 5, 7, 9 and dl= 2, 5, 10 μm were assumed for the number of ternary layers and the thickness of the defect layer, respectively. TiN is a metal-semiconductor composed of Titanium and Nitrogen. This chemical compound is used as a resilient coating on the surfaces of sensors due to its favorable optical properties, mechanical strength, exclusive electronic properties, and structural robustness [35]. An obtained state will be optimal if the obtained mode has a higher height, a sharper width, and a band gap with maximum width. Below, we will check the results obtained for different N and dm to find the optimal state for these variables. To carry out this research, we consider 0.0001 accuracy in all three cases. [36-38] The refractive index of hemoglobin was considered 1.380 and 1.365 in wavelength range 820 to 1300 nm [21, 39].

B. *Results of structure 1*

Fig. 2 represents the intensity of transmitted light of TiN/m/Ti O_2 structure for a different number of periods N.

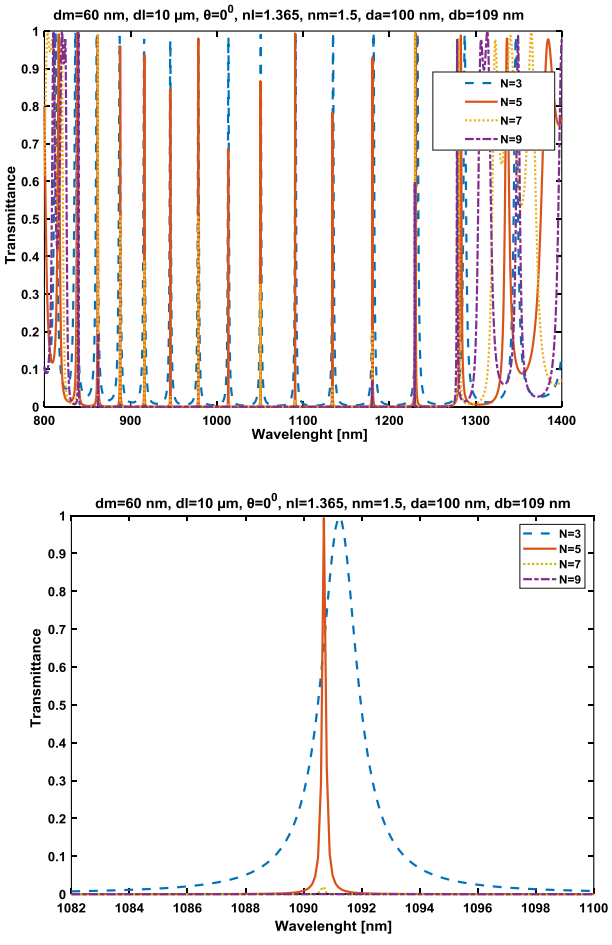

Fig. **2** Optimizing the number of periods (N) concerning wavelength. a: The effect of the number of triple layers (N), b: The height and width of the peaks

The result of Fig. 2 and numerical calculations shows that the system has a good bandgap width, and N=5 is the optimum state. Because at this value, the optimal situation is that more height and sharper width, and a band gap with maximum width are possible. Fig. 3 shows the transmitted light intensity for different values of dl =2 , 5 and 10 μm.

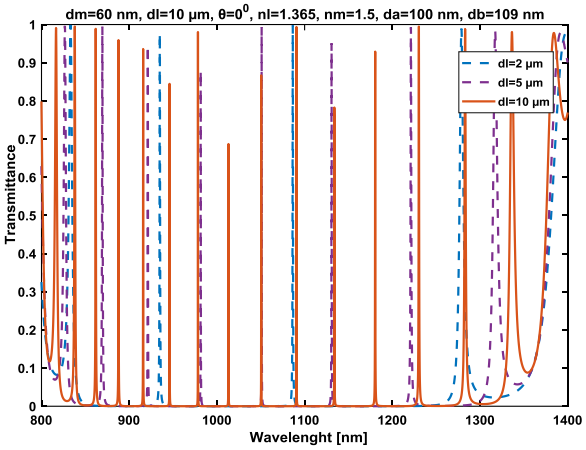

Fig. **3** Transmitted light intensity for dl =2 , 5 and 10 μm

Figure. 3 shows that the number of modes increases and the intensity of some modes decreases with increasing defect layer thicknesses. Table 1 shows the numerical calculations for different values of dl for the refractive index of hemoglobin. The parameters RW and $S_R = \frac{S}{RW}$ are the wavelengths of the peak of the defect mode (resonant wavelength) and relative or dimensionless sensitivity, respectively.

Table **1** Numerical calculations for dl = 2 , 5 and 10 μm for hemoglobin (structure 1).

$dl(\mu m)$	RW (nm)	S (nm /RIU)	S_R	FOM (1/RIU)
2	1087.0	546.7	0.53	364.5
5	1051.0	698.3	0.69	465.5
10	1091.0	780.0	0.73	780.0

As it is clear that, dl=10 μm is optimal due to the appropriate peak size and considering other effective components (band gap, width, sensitivity, etc.). The table denotes that dl=10 μm has optimum sensitivity (S=780.0 nm/RIU), relative sensitivity (S_R=0.729) and figure of merit (FOM=780.01/RIU) at resonance wavelength RF=1091.0 nm respectively. Fig. 4 shows the results obtained with different light incident angles θ. According to the previous sections, here we also calculated the results numerically.

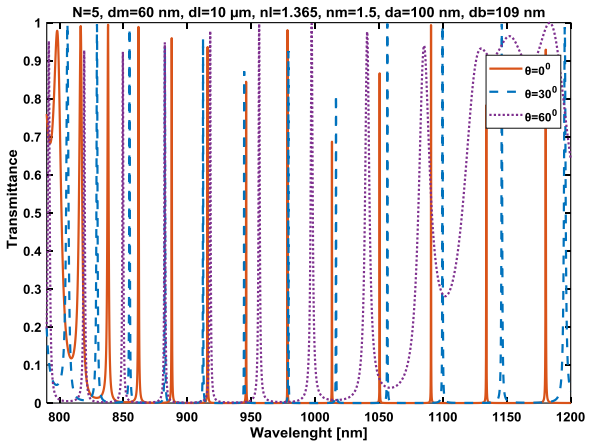

Fig. **4** Transmitted light intensity for $\theta = 0^0$, 30^0, 60^0 degrees

As the angle increases, the width of the modes increases, such that at an angle of 60 degrees, a small band gap with wide modes is produced. By examining these results, θ=0° is the most optimal possible mode. While the light incident is tuned to $\theta = 0^0$, the structure has a vast band gap and narrow, sharp modes. It can be observed from Fig. 5 that minor changes in the refractive index of hemoglobin can appropriately shift the mode.

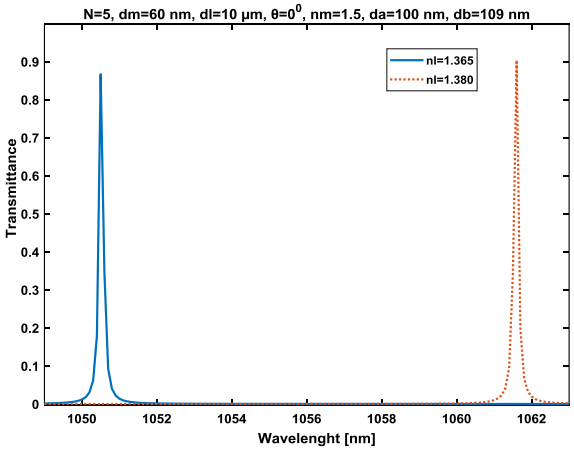

Fig. **5** Mode shifts of biosensor in two different hemoglobin refractive indices (nl)

In this part of the work, the effect of the refractive index of the middle layer (nm) is investigated. For comparison, we considered the values of 1, 1.5, 2, and 2.5.

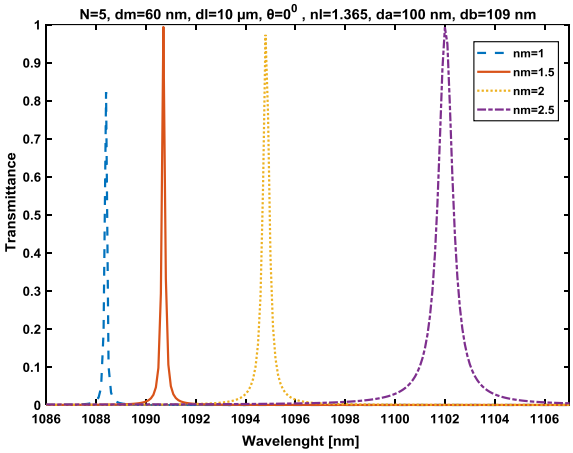

Fig. **6** Transmitted light intensity for different refractive indices of the middle layer (nm)

Figure. 6 shows that the glass layer (nm=1.5) is the most optimal possible state. On the other hand, the structure could be practically fabricated based on glass, and such a structure would be easier to access scientifically. In Fig. 7, we considered the thicknesses of the middle layer values of 0, 60, and 120 nm.

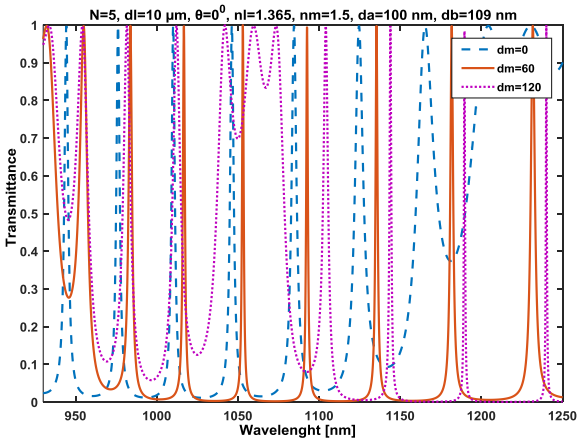

Fig. **7** The effect of thicknesses of the middle layer (dm)

Our analysis shows that dm = 60 is the most optimal state. According to the obtained results, the important parameters such as the width of the band gap, FWHM, resonance wavelength, quality factor, sensitivity, and FOM are 466.8 nm, 2 nm, 1181 nm, 590.5, 800 nm/RIU and 400, respectively.

C. *structure 2*

In this section, instead of layer a (TiN), in the first section, the $Al_XGa_{1-X}N$ layer was replaced. Aluminum Gallium Nitride is a III-Nitride semiconductor. This process alters the chemical composition by changing the ratios of aluminum (Al), gallium (Ga), and nitrogen (N). This flexibility allows for the tuning of its optical and electronic properties. The visual characteristics of $Al_xGa_{1-x}N$ semiconductor quantum dots can be altered by varying the composition percentages of Al and Ga. Introducing these quantum dots into the biosensor can allow for the modification of optical characteristics, thereby enhancing key biosensor features such as sensitivity, figure of merit, and quality factor. The obtained state ($Al_XGa_{1-X}N$/m/ TiO_2) will be optimal if the obtained mode has a higher height, a sharper width, and a band gap with the maximum width [40-42].

D. *Results of structure 2*

The important parameters in this section that should be determined are the fraction of aluminum composition (x), and some important parameters were investigated in section B. First, we examined the changes of x for x=0, 0.4, 0.8, and 1. Fig. 8 shows that a band gap only in the case of x=1 is suitable and wider than other values, because the peak corresponding to this value is narrower and the mode is thinner.

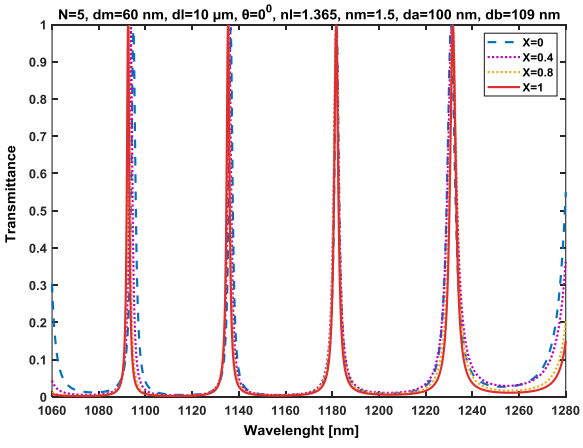

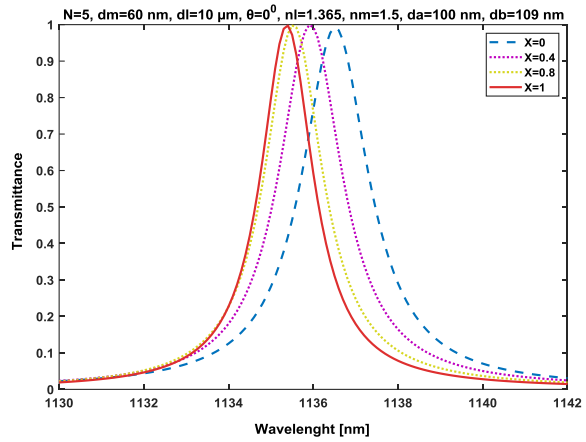

Fig. **8** (a) Transmittance for different values of aluminum fraction (x). (b) Shifts of modes by changing the aluminum fraction x

Figure. 9 shows the transmission spectrum of the biosensor concerning the thickness of the defect layer. In this structure, such as structure 1, it is clear that dl=10μm is the suitable selection, as shown in Fig. 9:

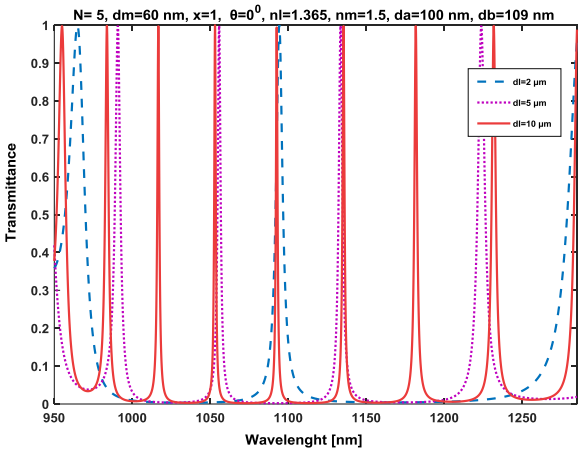

Fig. **9** Intensity of light passing through the biosensor according to the thickness of different defect layers

Figure. 10 shows some optimized modes located at approximately 1055 and 1095 nm. These modes have appropriate intensity and FWHM for detection purposes.

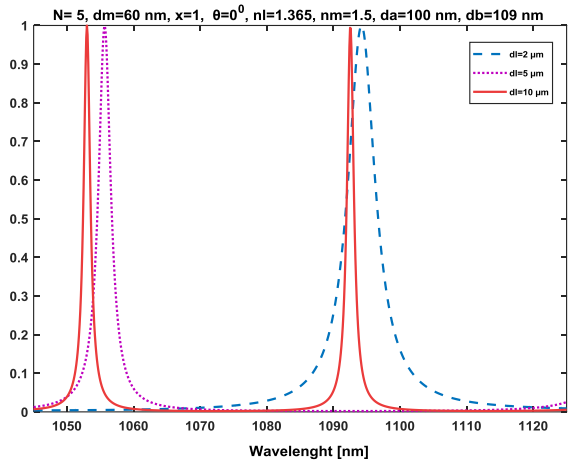

Fig. **10** Some optimized local modes in dl=10 μm.

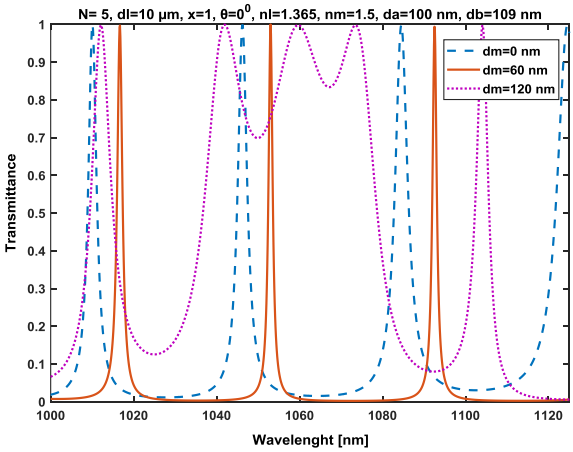

Fig. **11** The effect of thicknesses of the middle layer (dm)

As can be deduced from Fig. 11, the 60 nm thickness is optimal for structure 2. Fig. 12 shows the intensity of light passing through the biosensor according to the hemoglobin refractive index.

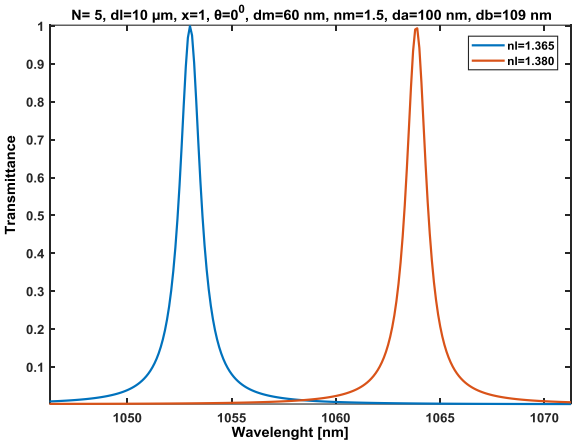

Fig. **12** the effect of thicknesses of the middle layer (dm)

Table 2 shows the numerical calculations for different values of dl for the refractive index of hemoglobin.

Table **2** Numerical calculations for dl = 2 , 5, 10 μm for hemoglobin (structure 2).

$dl(\mu m)$	RF (nm)	S $(nm$ /RIU)	S_R	FOM (1/RIU)
2	1094.0	600.0	0.55	300.0
5	1134.0	733.3	0.64	183.3
10	1135.0	800.0	0.70	400.0

Figure 13 shows the comparison of sensitivity and FOM values for different thicknesses of the two structures.

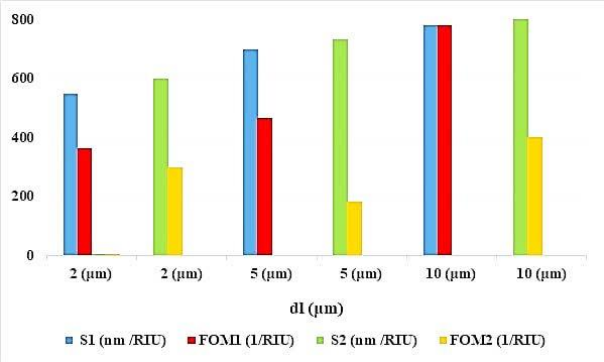

Fig. **13** The comparison of sensitivity and FOM values for different thicknesses of two structures.

The simulated biosensor exhibits sensitivity to refractive index variations of hemoglobin through apparent variations in the bandgap region, mode characteristics, and value of detection parameters. We have analyzed articles from various references to evaluate and compare the results obtained from the proposed structure. Table 3 demonstrates the sensing performance parameters of our biosensor compared to those reported in previous studies in wavelength range (WR).

Table 3. Assessing the sensitivity of the suggested sensor in comparison to other biosensing designs.

WR(nm)	S (nm /RIU)	FOM (1/RIU)	REFERENCE)
800-1200	46.51	-	[16]
2300-3100	6480	-	[18]
1630-1644	323	517	[17]
590-650	167	0.63	[20]
480-1800	1962	10916	[7]
950-1300	800	400	THIS WORK

Discussions

In this paper, we have established the theoretical studies of the ternary 1D-photonic crystal biosensor that enables enhanced sensitivity to small changes in the refractive index, to detect hemoglobin. Based on the presented findings, the proposed method has several advantages, including the ability to facilitate detection by increasing performance parameters, selecting optimal mode heights, and observing the effects of quantum dots, gallium nitride. Two similar structures were investigated, which, by using quantum dots instead of TiN layers, increased the sensitivity. Investigation shows that the photonic band gaps have sharp and suitable detection modes. This structure has suitable performance parameters such as Sensitivity, Figure of Merit, and Wavelength Ranges of 800 nm/RIU, 400, and 950 -1350 nm, respectively. We distinguished two hemoglobin samples. These efforts will advance future research and enhance knowledge in this field.

REFERENCES

[1] John, S. "Localization of light: Theory of photonic band gap materials," in Photonic band gap materials. Springer. pp. 563-665, 1996.

[2] CM, B. "Development and application of materials exhibiting photonic band gaps," J. Opt. Soc. Am. B, vol. **10**, pp. 280-413, 1993.

[3] John, S., H. Sompolinsky, and M.J. Stephen, "Localization in a disordered elastic medium near two dimensions," Physical Review B, vol. **27**, pp. 5592, 1983.

[4] Ďuriška, L., et al., Aqueous corrosion of aluminum-transition metal alloys composed of structurally complex phases: A review. Materials, 2021. **14**(18): p. 5418.

[5] Ghasemi, F. and S. Razi, Novel photonic bio-chip sensor based on strained graphene sheets for blood cell sorting. Molecules, 2021. **26**(18): p. 5585.

[6] Kong, W., et al., Wavelength manipulation in a grating metasurface loaded Bloch surface wave structure. Results in Physics, 2021. **27**: p. 104496.

[7] Firouzi, F., A. Vahedi, and S. Hagipour, Ternary one-dimensional photonic crystal biosensors for efficient bacteria detection: Role of quantum dots and material combinations. Physica B: Condensed Matter, 2025. **698**: p. 416766.

[8] Daher, M.G., et al., Design of a novel optical sensor for the detection of waterborne bacteria based on a photonic crystal with an ultra-high sensitivity. Optical and Quantum Electronics, 2022. **54**(2): p. 108.

[9] Taya, S.A., et al., Highly sensitive nano-sensor based on a binary photonic crystal for the detection of mycobacterium tuberculosis bacteria. Journal of Materials Science: Materials in Electronics, 2021. **32**: p. 28406-28416.

[10] Mohamed, A.M., et al., Design of a 1D PhC biosensor with enhanced sensitivity based on useful features provided for the detection of waterborne bacteria. Optical and Quantum Electronics, 2024. **56**(3): p. 433.

[11] Aly, A.H., et al., MATLAB simulation based study on poliovirus sensing through one-dimensional photonic crystal with defect. Scientific Reports, 2023. **13**(1): p. 9422.

[12] Meradi, K.A., et al., Optical biosensor based on enhanced surface plasmon resonance: theoretical optimization. Optical and Quantum Electronics, 2022. **54**(2): p. 124.

[13] Malek, C., et al., High performance biosensor composed of 1D defective photonic crystal for sensing and detection of distinguished blood components. Optical and Quantum Electronics, 2023. **55**(3): p. 196.

[14] Qu, W., et al., Application of Optical Fiber Sensing Technology and Coating Technology in Blood Component Detection and Monitoring. Coatings, 2024. **14**(2): p. 173.

[15] Su, M., et al., Tamm-plasmon-polariton biosensor based on one-dimensional topological photonic crystal. Results in Physics, 2023. **48**: p. 106454.

[16] El-Khozondar, H.J., et al., Design of one dimensional refractive index sensor using 40

[17] ternary photonic crystal waveguide for plasma blood samples applications. Physica E: Low-dimensional Systems and Nanostructures, 2019. **111**: p. 29-36.

[18] Goyal, A.K. and S. Pal, Design analysis of Bloch surface wave based sensor for haemoglobin concentration measurement. Applied Nanoscience, 2020. **10**: p. 3639-3647.

[19] Hao, J.-J., et al., Research on low-temperature blood tissues detection biosensor based on one-dimensional superconducting photonic crystal. Communications in Nonlinear Science and Numerical Simulation, 2020. **89**: p. 105299.

[20] Goyal, A.K., Design analysis of one-dimensional photonic crystal based structure for hemoglobin concentration measurement. Progress In Electromagnetics Research M, 2020. **97**: p. 77-86.

[21] Abadla, M.M. and H.A. Elsayed, Detection and sensing of hemoglobin using one-dimensional binary photonic crystals comprising a defect layer. Applied optics, 2020. **59**(2): p. 418-424.

[22] Abohassan, K.M. and H.S. Ashour, Demultiplexers for DWDM applications using one-dimensional planar binary photonic crystals defected with ZnS x Se1-x ternary alloys. Journal of Nanophotonics, 2022. **16**(1): p. 016006-016006.

[23] Abohassan, K.M., H.S. Ashour, and M.M. Abadla, A 1D binary photonic crystal sensor for detecting fat concentrations in commercial milk. RSC Advances, 2021. **11**(20): p. 12058-12065.

[24] Yashaswini, P.R., et al., Design and simulation of a highly sensitive one-dimensional photonic

crystal for different chemical sensing applications. Results in Optics, 2023. **11**: p. 100376.

[25] Ashour, H.S., K.M. Abohassan, and M.M. Abadla, Defective 1D quinary photonic crystal sensors for the detection of cancerous blood cells. Optical Engineering, 2021. **60**: p. 127106 - 127106.

[26] Al-Dossari, M., et al., Bio-Alcohol Sensor Based on One-Dimensional Photonic Crystals for Detection of Organic Materials in Wastewater. Materials, 2022. **15**(11): p. 4012.

[27] Kuliešaitė, M., et al., Partially coherent UV–VIS light generation in photonic crystal fiber using femtosecond pulses. Results in Physics, 2021. **31**: p. 104965.

[28] Mostafa, T., A. Ahmed, and E.-S. El-Rabie, Photonic crystal analog to digital converter a literature review, challenges, and some novel trends. Menoufia Journal of Electronic Engineering Research, 2022. **31**(2): p. 64-74.

[29] Rao, D.G.S., S. Swarnakar, and S. Kumar, Design of photonic crystal based compact all-optical 2× 1 multiplexer for optical processing devices. Microelectronics Journal, 2021. **112**: p. 105046.

[30] Zaky, Z.A. and A.H. Aly, Gyroidal graphene/porous silicon array for exciting optical Tamm state as optical sensor. Scientific Reports, 2021. **11**(1): p. 19389.

[31] Mohammed, N.A., et al., Tuberculosis biomedical sensor based on on-chip nanocavity 2D photonic crystal with high sensitivity and quality factor. Measurement, 2023. **222**: p. 113595.

[32] Patel, S.K., et al., Design of graphene metasurface based sensitive infrared biosensor. Sensors and Actuators A: Physical, vol. **301**, pp. 111767, 2020.

[33] Ramanujam, N., et al., Design of one dimensional defect based photonic crystal by composited superconducting material for bio sensing applications. Physica B: Condensed Matter, vol. **572**, pp. 42-55, 2019.

[34] White, I.M. and X. Fan, On the performance quantification of resonant refractive index sensors. Optics express, vol. **16**, pp. 1020-1028, 2008.

[35] Marmarou, A., et al. In vivo measurement of brain water by MRI. in Brain Edema VIII: Proceedings of the Eighth International Symposium, Bern, June 17–20, 1990. 1990. Springer.

[36] Del Villar, I., et al., Nano-Photonic Crystal D-Shaped Fiber Devices for Label-Free Biosensing at the Attomolar Limit of Detection. Adv Sci (Weinh), 2024. **11**(35): p. e2310118.

[37] Shaban, M., et al., Tunability and sensing properties of plasmonic/1D photonic crystal. Scientific reports, 2017. **7**(1): p. 41983.

[38] Panda, A. and P.D. Pukhrambam, Investigation of defect based 1D photonic crystal structure for real-time detection of waterborne bacteria. Physica B: Condensed Matter, 2021. **607**: p. 412854.

[39] Wang, P., et al., MXene/metal–organic framework based composite coating with photothermal self-healing performances for antifouling application. Chemical Engineering Journal, 2023. **474**: p. 145835.

[40] Chakaya, J., et al., The WHO Global Tuberculosis 2021 Report–not so good news and turning the tide back to End TB. International Journal of Infectious Diseases, 2022. **124**: p. S26-S29.

[41] Aly, A.H., et al., Novel biosensor detection of tuberculosis based on photonic band gap materials. Materials Research, 2021. **24**: p. e20200483.

[42] Altug, H., et al., Advances and applications of nanophotonic biosensors. Nature nanotechnology, vol. **17**, pp. 5-16, 2022.

[43] Lazareva, E.N. and V.V. Tuchin, "Measurement of refractive index of hemoglobin in the visible/NIR spectral range," Journal of biomedical optics, vol. **23**, pp. 035004-035004, 2018.